

An Investigation of the Mechanical Behavior of Carbon Epoxy Cross Ply Cruciform Specimens Under Biaxial Loading

Andreas Makris,¹ Carla Ramault,¹ Danny Van Hemelrijck,¹ Dimitrios Zarouchas,¹ Ebrahim Lamkanfi,² Wim Van Paepgem²

¹Department of Mechanics of Materials and Constructions, Vrije Universiteit Brussel, Brussels, Belgium

²Department of Materials Science and Engineering, Ghent University, Ghent, Belgium

In this study, carbon epoxy cruciform type specimens with a cross-ply layup were biaxially and uniaxially in-plane loaded using four independent servo-hydraulic actuators. Four different biaxial loading ratios were investigated when the applied load was quasi-static. A comparison between experimental observations (for the damage and strain evolution of the biaxially loaded central section of the specimen) coming from digital image correlation measurements and a 3D finite element damage model will be shown. The symmetry and the uniformity of the strain field on the biaxially loaded zone were by the use of digital image correlation measurements investigated. Furthermore, the failure loads coming from the load cells of the machine were straightforward compared with the output of the finite element damage model. POLYM. COMPOS., 31:1554–1561, 2010. © 2009 Society of Plastics Engineers

INTRODUCTION

The lack of reliable multiaxial or even biaxial experimental data to validate failure theories is a critical step in the evolution and a most efficient usage of composite materials [1]. Because of the complex anisotropic behavior of composite materials more advanced experimental testing is needed. The current practice of using uniaxial test results to predict failure for multiaxial stress states seems inadequate. To study the mechanical behavior of fiber reinforced polymeric matrix composite laminates under static and cyclic in-plane complex stress states a horizontal biaxial loading frame and a special cruciform type specimen have been developed. The reliability of the experimental failure data depends a lot on the proper design of the cruciform specimen and the accuracy of the

measurements [2]. The specimen should fulfill some requirements as failure must mainly occur in the biaxially loaded centre and the strain distribution should also be uniform. Smits et al. [3] proposed a geometry to satisfy these requirements. In this study, the evolution of the strain and damage of the biaxially loaded central section of this common used cruciform geometry [4, 5] was experimentally and numerically investigated. In the numerical part a progressive damage modeling (PDM) technique was implemented in the commercial finite element software Ansys© to simulate the biaxial mechanical test and study the damage evolution. Among literature, one of the first progressive damage models present was introduced by Chou et al. [6], where no distinction between different failure modes was considered. In more recent literature, Tserpes et al. [7, 8] presented a 3D model for predicting residual strength, final failure load, and modes in bolted composite joints under quasi-static tensile loading by using a set of 3D discrete failure criteria representative for the basic failure modes of composite materials.

EXPERIMENTAL PART

Plane Biaxial Test Bench for Testing Cruciform Specimens

The developed biaxial test rig, see Fig. 1, has a capacity of 100 kN in each perpendicular direction, but only in tension, limiting the experimental results to the first quadrant of the 2D stress space failure envelope. This type of machine is often used to perform mechanical biaxial tests of composite materials or metals [9–11]. As no cylinders with hydrostatic bearing were used, failure or slip in one arm of the specimen will result in sudden radial forces, which could seriously damage the servo-hydraulic cylinders and load cells. To prevent this, hinges were used to connect the servo-hydraulic cylinders to the

Correspondence to: A. Makris; e-mail: amakris@vub.ac.be

DOI 10.1002/pc.20943

View this article online at wileyonlinelibrary.com.

© 2009 Society of Plastics Engineers

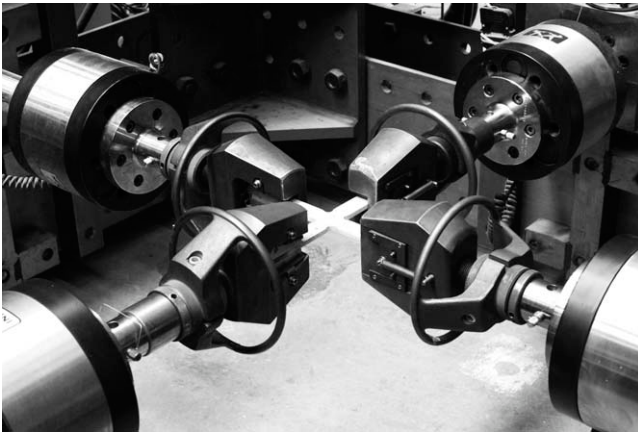


FIG. 1. Plane biaxial test device for testing cruciform specimens.

test frame. By using four hinges in each loading direction results in an unstable situation in compression and, consequently, only tension loads can be applied. The stroke of each cylinder is 150 mm, while the loading may be static or dynamic up to a frequency of 20 Hz. Moreover, each cylinder is independently controlled, and any type of loading waveform, including spectral sequences of variable amplitude, can be efficiently introduced using the dedicated software and control system.

Cruciform Specimen and Mechanical Properties of the UD Material

Specimens tested were manufactured using carbon UD SE84 prepreg material. The layup used for this study was $[(0/90)_2, (90/0)_2]_{sym}$, the thickness of each lamina was 0.28 mm, the width of the arms was 25 mm, and the length 250 mm. This leads to a total nominal thickness of 4.48 mm for the arms of the cruciform specimen and of 2.24 mm for the biaxially loaded zone, where one group of $[(0/90)_2]$ was milled away at each side of the specimen, see Fig. 2. To reduce interlaminar stresses, the layup was built up in a way that the top layer of the milled zone and the 4th or 13th layer of the arms have the same orientation (90°), this modification proved to improve the failure behavior of glass epoxy specimens under biaxial

loading conditions [12]. A speckle pattern was also applied on the surface of the specimen to perform optical measurements using the Digital Image Correlation Technique [13].

To obtain the elastic properties and strength of the UD material, mechanical tests were realized. Average five specimens per property were tested. For the uniaxial tensile properties, ISO-527-5 coupons were used, for the uniaxial compression properties ISO-14126, and all shear properties were measured by using the Iosipescu method (ASTM D5379). For generating through-thickness (TT) data in both tension and compression the circular-waisted block (CWB), [14] testing method was used. In Table 1, the average values and standard deviation of the elastic properties of the UD SE84 material can be found. These properties together with the strength of the lamina, see Table 2, were used as basic input for the FEDM.

In Table 1, defining term's indexation, "123" is the fiber coordinate system, "1" is the fiber direction, "2" is the direction transverse to the fibers, and "3" is the through thickness direction.

In Table 2, X_T, X_C are the tensile and compressive strength longitudinal to the fibers, Y_T, Y_C are the tensile and compressive strength transverse to the fibers normal to "13" plane, Z_T, Z_C are the tensile and compressive strength transverse to the fibers normal to "12" plane, while $S_{ij}, i, j = 1, 2, 3$, is the shear strength of the lamina.

Strain Measurements Using Digital Image Correlation Technique

To be able to study the symmetry of the strain field and the occurring shear strains experimentally, full field methods are necessary. Strain measurements using a strain gage or extensometer are not sufficient, because both give an average value of the deformation along their gauge length and sometimes fail earlier than the specimen.

The strain field of glass epoxy specimens of the same geometry under uniaxial or biaxial loading conditions was in a previous study extensively investigated [2]. There, because of the complexity of the specimen's geometry, different measurement techniques (Strain gages,

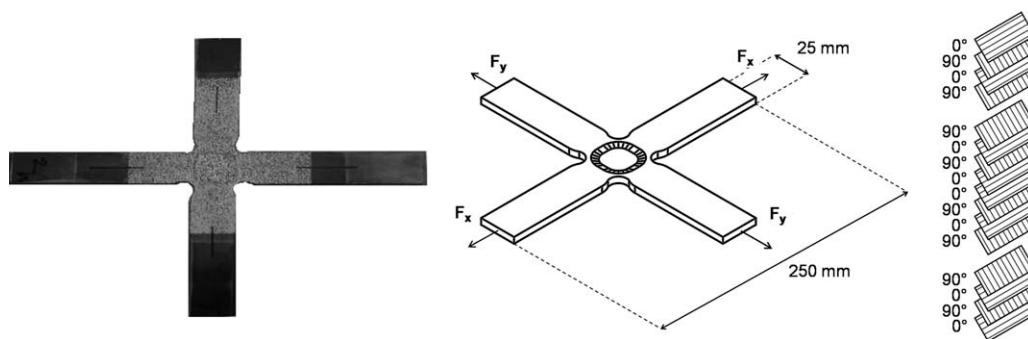


FIG. 2. Cruciform geometry.

TABLE 1. Elastic properties of the UD SE84 carbon lamina.

	E_1 (GPa)	E_2 (GPa)	E_3 (GPa)	G_{12} (GPa)	G_{23} (GPa)	G_{13} (GPa)	ν_{12}	ν_{23}	ν_{13}
Average	124.3	8.14	7.8	4.49	2.44	3.93	0.32	0.505	0.34
SD	4.4	0.1	0.12	0.07	0.21	0.1	0.02	0.005	0.025

Digital Image Correlation (DIC) and Electronic Speckle pattern Interferometry (ESPI) techniques were used combined or separately) were applied to investigate strain concentrations, obtain the valid strain field of the zone of interest, and finally, ensure the accuracy of the measurements.

In this study, Digital Image Correlation Technique (DICT) was used to follow the strain evolution of the areas of interest. DICT is an experimental technique, which offers the possibility to determine in-plane and out of plane displacement and deformation fields of the surface of objects under any kind of loading, based on a comparison between images taken at different load steps. By deriving the displacement field, the desirable strain field can be obtained.

Four different load ratios (F_x/F_y) were applied on cruciform specimens (three different biaxial cases 1/1, 2/1, 3/1, and a uniaxial case 0/1), and for each ratio, two specimens were tested in tension until total failure. Biaxial testing of cruciform specimens was performed using load control of the machine with a constant load speed of 5 kN/min and uniaxial testing of them by displacement control with a displacement rate of 1 mm/min. Below, in Fig. 3, presented is the first quadrant of the failure envelope for the cross-ply cruciform laminate in strain space from measurements coming from the geometrical centre of the central section.

NUMERICAL PART

Progressive Damage Modeling

A three dimensional finite element model was developed using the commercial software Ansys to compare with experimental observations and understand better the different failure mechanisms. The model is using a progressive damage scenario. Progressive damage modeling (PDM) technique has four basic steps, (i) stress analysis of the structure, (ii) failure analysis in an element basis, (iii) degradation of the properties of the failed elements,

and (iv) application of a total failure criterion. The procedure stops when the total failure occurs, which physically means that the structure cannot take any additional load. In this study, and to simulate the testing of the cruciform specimen, stress analysis was done by using Ansys solver. For the failure analysis, different failure modes were considered, namely, matrix tensile and compressive cracking, fiber tensile and compressive failure, fiber-matrix shear out and out of plane failure. These failure modes represent basic failure modes of the composite materials. For the detection of the failure modes, a set of 3D stress-based polynomial failure criteria was used, Eq. 1–7. The specific set of failure criteria has been proposed in Refs. 7 and 15 in which it has been successfully used for analyzing failure of composite bolted joints subjected to tensile loading.

Matrix tensile cracking, for $\sigma_{22} > 0$:

$$\left(\frac{\sigma_{22}}{Y_T}\right)^2 + \left(\frac{\sigma_{12}}{S_{12}}\right)^2 + \left(\frac{\sigma_{23}}{S_{23}}\right)^2 \geq 1 \quad (1)$$

Matrix compressive cracking, for $\sigma_{22} < 0$:

$$\left(\frac{\sigma_{22}}{Y_C}\right)^2 + \left(\frac{\sigma_{12}}{S_{12}}\right)^2 + \left(\frac{\sigma_{23}}{S_{23}}\right)^2 \geq 1 \quad (2)$$

Fiber tensile failure, for $\sigma_{11} > 0$:

$$\left(\frac{\sigma_{11}}{X_T}\right)^2 + \left(\frac{\sigma_{12}}{S_{12}}\right)^2 + \left(\frac{\sigma_{13}}{S_{13}}\right)^2 \geq 1 \quad (3)$$

Fiber compressive failure, for $\sigma_{11} < 0$:

$$\left(\frac{\sigma_{11}}{X_C}\right)^2 \geq 1 \quad (4)$$

Fiber-matrix shear out, for $\sigma_{11} < 0$:

$$\left(\frac{\sigma_{11}}{X_C}\right)^2 + \left(\frac{\sigma_{12}}{S_{12}}\right)^2 + \left(\frac{\sigma_{13}}{S_{13}}\right)^2 \geq 1 \quad (5)$$

TABLE 2. Strength of the UD SE84 carbon lamina.

	X_T (MPa)	X_C (MPa)	Y_T (MPa)	Y_C (MPa)	Z_T (MPa)	Z_C (MPa)	S_{12} (MPa)	S_{23} (MPa)	S_{13} (MPa)
Average	2751	1180	25	162	42	165	106.9	35.21	97.87
SD	32	53	2.5	2	2.5	2.5	2.78	3.93	5.2

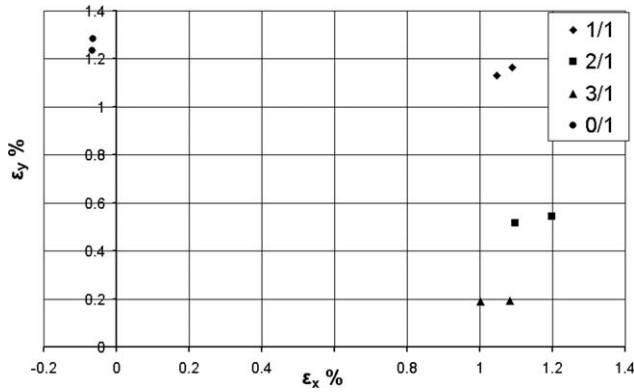


FIG. 3. First quadrant of the failure envelope of the cross ply laminate.

Out of plane failure, for $\sigma_{33} > 0$:

$$\left(\frac{\sigma_{33}}{Z_T}\right)^2 + \left(\frac{\sigma_{13}}{S_{13}}\right)^2 + \left(\frac{\sigma_{23}}{S_{23}}\right)^2 \geq 1 \quad (6)$$

Out of plane failure, for $\sigma_{33} < 0$:

$$\left(\frac{\sigma_{33}}{Z_C}\right)^2 + \left(\frac{\sigma_{13}}{S_{13}}\right)^2 + \left(\frac{\sigma_{23}}{S_{23}}\right)^2 \geq 1 \quad (7)$$

Numerators in *Eqs. 1–7* (σ_{ij}) represent the element-stress components, while the denominators the corresponding strength of the lamina, both referring to the fiber coordinate system.

Material properties degradation was performed in an element basis. This means that each time a specific failure mode was satisfied for an element, then its elastic properties were being degraded properly according to degradation rules. Different degradation factors were used for matrix failure, fiber failure, fiber-matrix shear out, and out of plane failure, see Table 3. The specific degradation scenario was used by Papanikos et al. [15] to model the damage progression of bonded carbon epoxy composite repairs on cracked metallic plates and in Ref. 7, where the influence of two different sets of failure criteria and degradation rules in the strength predictions of bolted composite joints was investigated. It has to be stated that most of the times these rules are empirical and include assumptions resulting from engineering constraints in the

TABLE 3. Degradation factors.

Failure mode	Material property degradation
Matrix tensile cracking	$E_{22}' = 0.2 * E_{22}, G_{12}' = 0.2 * G_{12}, G_{23}' = 0.2 * G_{23}$
Matrix compressive cracking	$E_{22}' = 0.4 * E_{22}, G_{12}' = 0.4 * G_{12}, G_{23}' = 0.4 * G_{23}$
Fiber tensile failure	$E_{11}' = 0.07 * E_{11}$
Fiber compressive failure	$E_{11}' = 0.14 * E_{11}$
Fiber-matrix shear out	$G_{12}' = v_{12}' = 0$
Out of plane failure, $\sigma_{33} > 0$	$E_{33}' = G_{13}' = G_{23}' = v_{13}' = v_{23}' \approx 0$
Out of plane failure, $\sigma_{33} < 0$	$E_{33}' = G_{13}' = G_{23}' = v_{13}' = v_{23}' \approx 0$

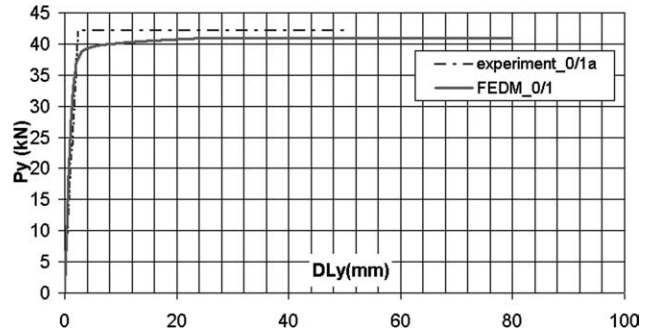


FIG. 4. Load-displacement graph for the edge of the specimen.

elastic properties of composite materials. In literature, details about definition and development of degradation rules can be found in Refs. 16 and 17.

Finally, a total failure criterion declares when the structure cannot take any additional load. It depends on the nature of the problem what can be considered as total failure. In the real biaxial experiment, total failure can be translated as the complete separation of one of the arms from the rest of the specimen. This can be observed in the simulation by following the displacement of an edge node of an arm when load control or by following the reaction force of an edge node when displacement control. The finite element model should converge to a disproportional increase of the displacement for the first case and to a constant load value for the second case. Below the Load-Displacement graph is plotted for the uniaxial case from the FEDM and from the experimental data, see Fig. 4. There the model converges to a constant value (41 kN failure load) close to the measured experimental value (42.14 kN) for test 0/1a.

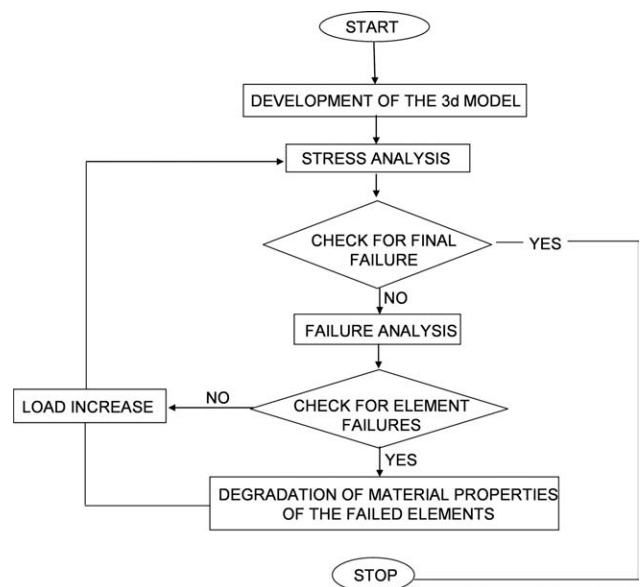


FIG. 5. Flowchart of the FEDM algorithm.

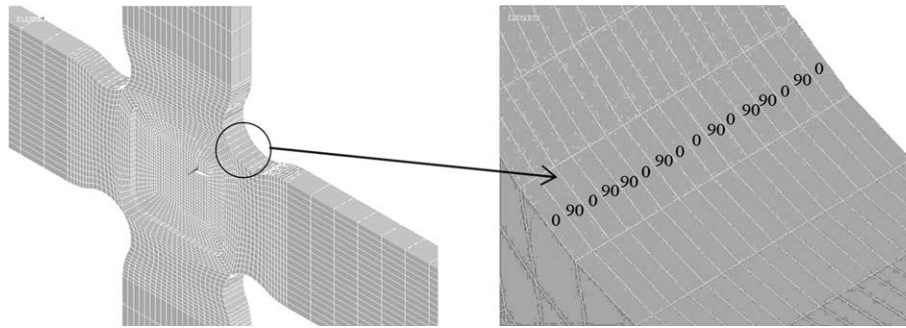


FIG. 6. Sixteen elements through thickness or one element/layer.

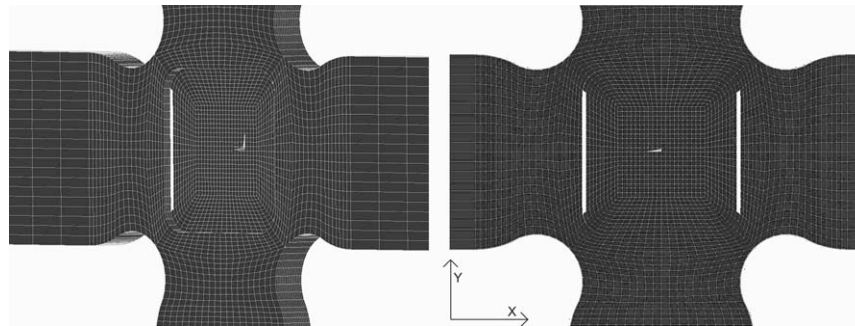


FIG. 7. Location of the damage initiation (white elements) for a cruciform specimen under $F_x = 6\text{kN}$ ($F_x/F_y = 2/1$) obtained from the finite element model.

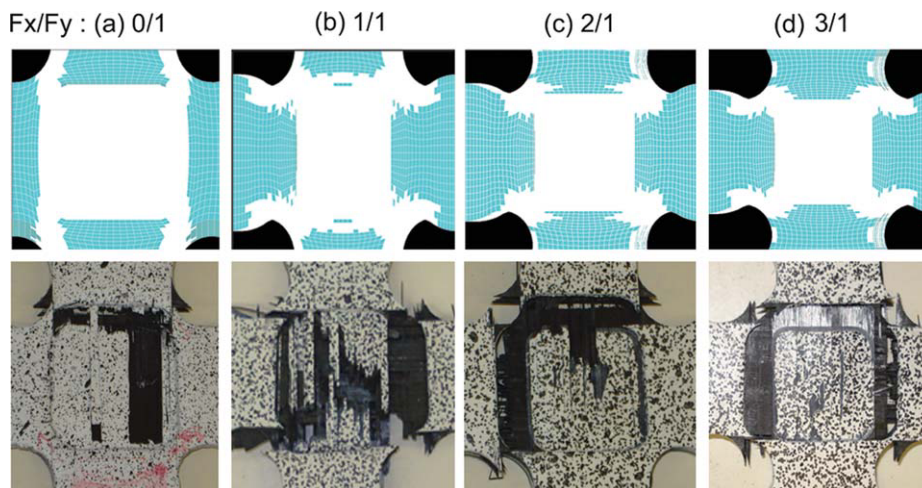


FIG. 8. Total failure locations from the experiments (below) and from the finite element damage model (above) for the four loading ratios. [Color figure can be viewed in the online issue, which is available at wileyonlinelibrary.com.]

TABLE 4. Total failure loads.

Biaxial ratio	Experiments		FEDM		FEDM vs. Experiments Variation (%)
	Failure F_x (kN)	Failure F_y (kN)	Failure F_x (kN)	Failure F_y (kN)	
1/1 a	42.10	42.16	43.00	43.00	2.09
1/1 b	40.50	40.71	43.00	43.00	5.81
2/1 a	44.41	22.21	42.00	21.00	5.75
2/1 b	42.35	21.17	42.00	21.00	0.82
3/1 a	37.78	12.59	40.00	13.33	5.54
3/1 b	37.57	12.52	40.00	13.33	6.08
0/1 a	0.00	42.14	0.00	41.00	2.77
0/1 b	0.00	42.40	0.00	41.00	3.41

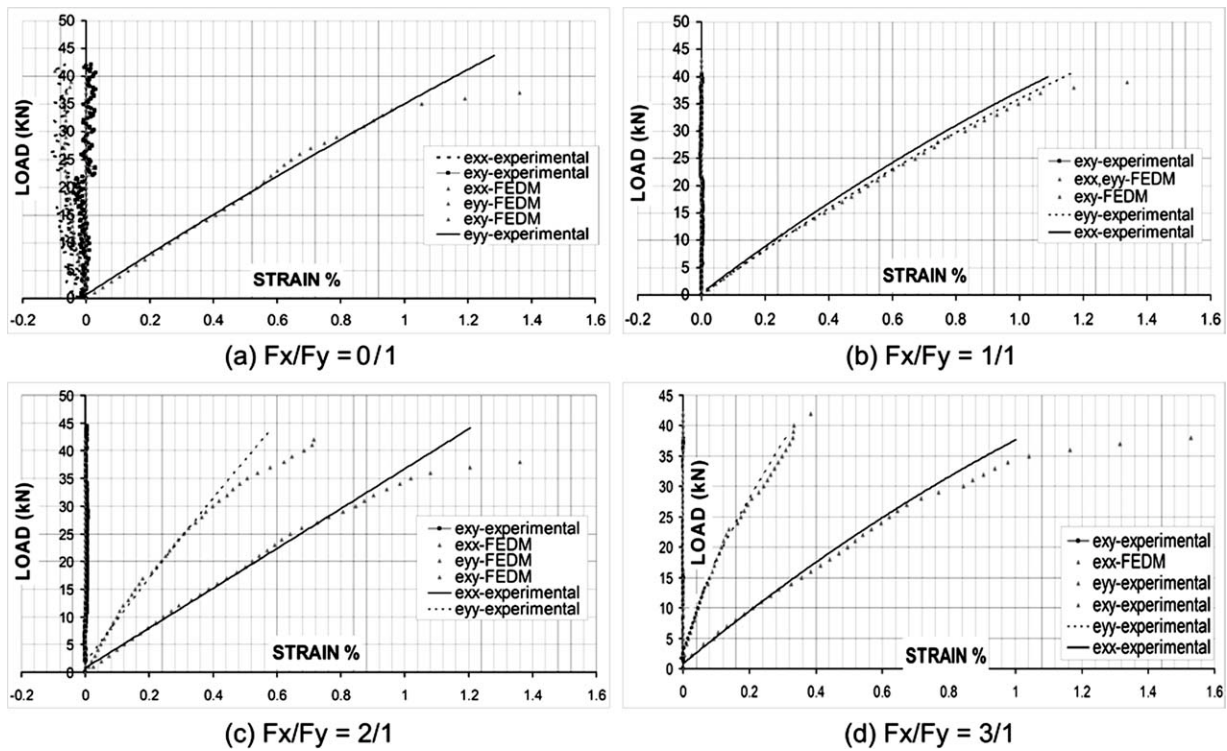


FIG. 9. A comparison between DIC measurements and the FEDM using the load-strain graphs for the four loading cases.

Flowchart of the Model

A computer program has been created using Ansys ©FE code [18] to implement the progressive damage technique and simulate the mechanical testing of the cruciform specimen. The geometry of the specimen was parametrically built, which allowed modifications of the

dimensions easily to be done. The program is explained by the flowchart shown in Fig. 5 and involves the following basic steps: (i) creation of the 3D model by giving as input the material properties, the geometry of the examined configuration, the boundary conditions, the initial load, and the load step, (ii) performing stress analysis

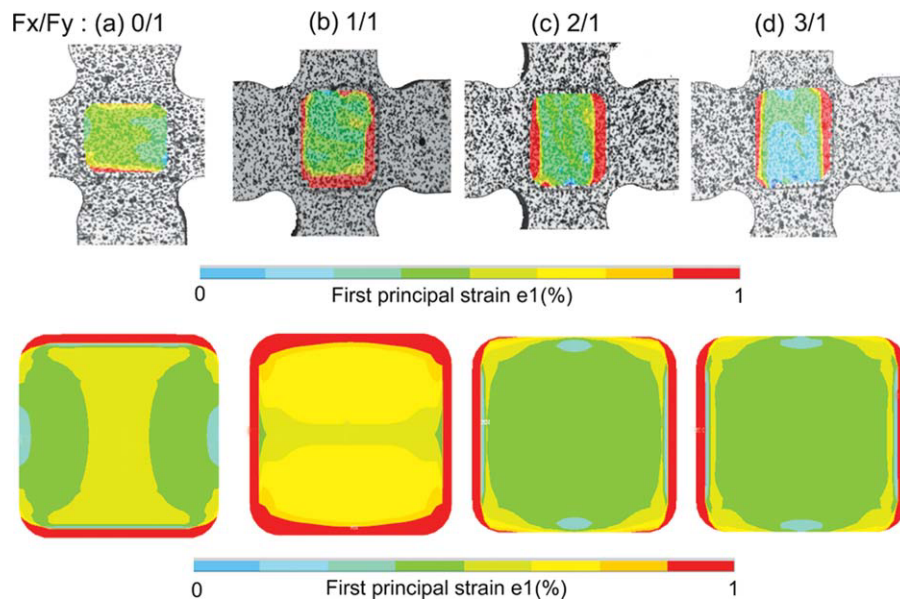


FIG. 10. First principal strain field for the four load cases obtained by i) DICT (above) ii) FEDM (below). [Color figure can be viewed in the online issue, which is available at wileyonlinelibrary.com.]

using Ansys® solver to calculate the stresses, (iii) check for final failure, (iv) performing failure analysis by applying the failure criteria, (v) check for element failures; if no failure is predicted, the applied load is increased by a pre-defined increment and the program returns to stress analysis; if a mode of failure is predicted in an element the program continues to the next step, (vi) degradation of material properties of the failed element, and (vii) increase load and return to stress analysis.

Cruciform Composite Geometry Modeling Using Solid Elements

For the 3D modeling of the specimen, “solid46” element type was selected [19]. Solid46 is an 8-node layered solid element, designed to model layered shells or solids, with three degrees of freedom at each node: translations in the nodal x, y, and z directions. For the cruciform modeling through thickness, one element corresponds to one layer, see Fig. 6. A total number of 62,080 elements were used to achieve a converged solution. As biaxial experiments were performed by load control of the machine and uniaxial by displacement control of it, the application of the load in the model was done by setting nodal forces in the arms of the cruciform specimen in the first case and nodal displacements in the second case.

COMPARISON BETWEEN FEDM AND EXPERIMENTAL OBSERVATIONS

Damage Initiation and Total Failure Loads

For the four loading cases according to the FEDM, failure initiated at an early loading stage. The value of the necessary load in the main loading direction to initiate damage mechanisms in the cruciform specimen was for all the tested cases ~14% of the total failure load. The initial failure mode detected was matrix cracking of the edge elements of the milled zone. In Fig. 7, the location of the failed elements is presented for the loading case $F_x/F_y = 2/1$, there the edge elements of the top layer (90°) of the milled zone (5th and 12th layer), were failed under $F_x = 6$ kN.

Figure 8 presents a comparison between the total failure locations as captured from the experiments and the one predicted from the simulations for the four different load ratios. The damaged elements according to the FEDM are presented in white. The locations where damage was concentrated were the corners and the milled zone of the specimen.

Finally, in Table 4 are compared the total failure loads as measured from the load cells of the biaxial machine with the output failure loads from the finite element program. The variation of the results was from 2% to 6%.

Strain Evolution of the Biaxially Loaded Zone

Figure 9 presents the load strain graphs from the four loading cases, for both FEDM and DICT measurements, from the centre of the specimen. Normal strain is plotted for both directions (e_{xx} , e_{yy}) and also the in-plane shear strain e_{xy} is shown. For all the loading cases, the occurring shear is negligible, and there is a good correlation between measurements and the FEDM.

A quantitative and a qualitative comparison between the first principal strain distribution coming from the DIC measurements and the finite element program is shown in Fig. 10. The data are plotted for 50% of the total failure of each loading case. Strain concentrations on the edge of the milled zone were observed, while the distribution of the strain for all the loading cases for the rest largest part of the biaxially loaded zone was uniform.

CONCLUSION

The strain and the damage evolution of carbon epoxy cross-ply specimens under biaxial loading conditions were studied. A numerical simulation for the biaxial test was developed and validated by experimental data coming from digital image correlation measurements (DIC) and failure loads measured from the load cells of the machine. The finite element model with a progressive damage scenario implemented showed good correlation with the experimental observations. Variation for the failure loads coming from the FEDM and the experiments was between 2 and 6%. Moreover, there was a good match, quantitative and qualitative, concerning the strain field of the central biaxially loaded section.

From the analysis of the strain data, strain concentrations on the edge of the milled zone were measured from DICT and calculated from the finite element program. Furthermore, undesirable premature damage outside the biaxially loaded milled zone was observed, therefore, to reduce these phenomena and further improve the accuracy of the test, an optimization of the shape of the cruciform specimen and a study of geometrical parameters such as corner radius, thickness, and shape of the milled zone is necessary. As objective function can be used, the uniformity of the central strain field and the concentration of the damage in the central biaxially loaded section. The 3D model, which was presented in this article and proved to produce reliable results, can be used as a simulation tool of the experiment to evaluate the outputs of the optimization method before manufacturing and testing real specimens.

ACKNOWLEDGMENTS

The authors would like to acknowledge the financial support for this research from the Fonds Wetenschappe-

lijk Onderzoek (FWO)—Vlaanderen, Belgium and also thank Mr. Frans Boulpaep for technical support including the manufacture and testing of the cruciform specimens.

REFERENCES

1. M.J. Hinton, A.S. Kaddour, and P.D. Soden, "Failure Criteria in Fiber Reinforced Polymer Composites: The World-Wide Failure Exercise," Elsevier (2004).
2. D. Van Hemelrijck, C. Ramault, A. Makris, E. Lamkanfi, W. Van Paepegem, and D. Lecompte, *Proc IME J Mater Des Appl.*, **222**, 231 (2008).
3. A. Smits, D. Van Hemelrijck, T.P. Philippidis, and A. Cardon, *Compos. Sci. Technol.*, **66**, 964 (2006).
4. Y. Yu, M. Wan, and X.D. Wu, *J. Mater. Process. Technol.*, **123**, 67 (2002).
5. J.S. Welsh and D.F. Adams, *Compos. A.*, **33**, 829 (2002).
6. S-C. Chou, O. Orringer, and J.H. Rainey, *J Compos. Mater.*, **11**, 834, (1977).
7. K.I. Tserpes, G. Labeas, P. Papanikos, and Th. Kermanidis, *Compos. B.*, **33**, 521 (2002).
8. K.I. Tserpes, P. Papanikos, and Th. Kermanidis, *Fatigue. Fract. Eng. Mat. Struc.*, **24**, 663 (2001).
9. J.P. Boehler, S. Demmerle, and S. Koss, *Exp. Mech.*, **34**, 1 (1994).
10. J.S. Welsh and D.F. Adams, *Exp. Mech.*, **40**, 312 (2000).
11. A. Makinde, L. Thibodeau, and K.W. Neale, *Exp. Mech.*, **32**, 138 (1992).
12. C. Ramault, A. Makris, D. Van Hemelrijck, and E. Lamkanfi, W. Van Paepegem, in Proceedings of the 17th International Conference on Composite Materials (ICCM17), *Edinburgh, Scotland*, 132 (2009).
13. M.A Sutton, J.J Orteu, and H.W Schreier, "Image Correlation for Shape Motion and Deformation Measurements," ISBN 978-0-387-78746-6, Springer, (2009).
14. W. R Broughton and G.D Sims, "NPL Report DMM (A) 148," Middlesex, United Kingdom, National Physical Laboratory, (1994).
15. P. Papanikos, K.I. Tserpes, G. Labeas, and Sp. Pantelakis, *Theoretic. Appl. Fract. Mech.*, **43**, 189 (2005).
16. K.I. Tserpes, P. Papanikos, and Th. Kermanidis, *Fatigue. Fract. Eng. Mat. Struc.*, **24**, 663 (2001).
17. P.P. Camanho and F.L. Matthews, *J. Compos. Mater.*, **33**, 906 (1999).
18. "ANSYS Users Manual, Version 6," Swanson Analysis Systems, Inc, (2002).
19. R.L Taylor, P.J. Beresford, and E.L. Wilson, *Int. J. Numeric. Methods. Eng.*, **10**, 1211 (1976).